

## On the generation of secondary microseisms observed in northern and central Europe

Heinz-Hermann Essen,<sup>1</sup> Frank Krüger,<sup>2</sup> Torsten Dahm,<sup>3</sup> and Ingo Grevemeyer<sup>4</sup>

Received 9 December 2002; revised 7 May 2003; accepted 21 May 2003; published 29 October 2003.

[1] Microseism recordings from four European broadband stations and from three seismic arrays in Scotland, Norway, and Germany are compared with model wave data of the oceanic wave field in the North Atlantic and local ocean wave data from the Norwegian coast at 60°N, both measured during February–March 2000. Two approaches have been tested to locate generation areas of microseismic energy: a new amplitude correlation technique and beam backprojection from the three seismic arrays. Both techniques reveal that the main generation areas are located in specific regions off the coast of Southwest Norway and North Scotland. Seismic stations distant from these generation areas record a superposition of seismic energy from different source regions. Those close to a specific source region also show a high correlation with it. Both techniques give upper limits for the extent of the generation area of the strongest storm on 6/7 March at the southwest Norwegian coast of about 500 km. By using marine X-band radar measurements of the two-dimensional wave height spectrum, we estimate that the relative change of the extension of the generation area off the coast of southwest Norway during several storms is less than a factor of 3. This indicates that the size of the generation area is controlled by static features as coastline or bathymetry, and not by the extent of the storms. Microseism energy appears to be mainly controlled by the wave height in distinct and identifiable generation regions, so that the wave climate in these regions can be studied using historical records of microseisms. *INDEX TERMS:* 4560 Oceanography: Physical: Surface waves and tides (1255); 7255 Seismology: Surface waves and free oscillations; 7299 Seismology: General or miscellaneous; *KEYWORDS:* ocean microseisms, generation mechanisms, generation areas, ocean wave data

**Citation:** Essen, H.-H., F. Krüger, T. Dahm, and I. Grevemeyer, On the generation of secondary microseisms observed in northern and central Europe, *J. Geophys. Res.*, 108(B10), 2506, doi:10.1029/2002JB002338, 2003.

### 1. Introduction

[2] Microseisms are recorded as the continuous background signal on seismic records with periods between 3 and 25 s. Periods between 12 and 25 s (frequencies between 0.04 and 0.15 Hz) are referred to as primary and periods between 3 and 13 s (frequencies between 0.08 and 0.3 Hz) as secondary microseisms and are often observed regionally as distinct spectral peaks with peak frequencies scaling relative to ocean surface waves like 1:2. Microseisms have been recorded since seismologists started to record the Earth's ground movements to detect earthquakes. *Wiechert* [1904] associated microseisms with ocean waves and coastal surf. *Gutenberg* studied microseisms over several decades [e.g., *Gutenberg*, 1912, 1921, 1936, 1947]. More recent studies update his work for central and northern Europe [*Szelwis*, 1982; *Darbyshire*, 1991; *Friedrich et al.*, 1998].

*Longuet-Higgins* [1950] formulated the first reliable theory about the generation of secondary microseisms, and *Hasselmann* [1963] explained the generation of primary microseisms. *Webb* [1992] and *Bromirski and Duennebie* [2002] investigated microseisms recorded by seismometers and pressure gauges within and under the seabed and onshore near the coast.

[3] Recently, microseisms have gained new attention in context with the discussion on decadal climate variability [*Bromirski et al.*, 1999]. Microseisms are generated by ocean surface waves and hence reflect the wave climate in the generation area. For the investigation of decadal climate variability, time series are needed which cover the period of the twentieth century, or even longer periods. In situ measurements of waves are generally not available before about 1970. In situ measurements of wind are available but are not homogeneous due to changes in the instruments used or insufficient spatial coverage. Time series of microseisms are homogeneous if they have been recorded at fixed positions with the same instruments, or with instruments for which the response to microseism ground movements is known. *Grevemeyer et al.* [2000], for example, took on the challenge and investigated the microseism activity in Hamburg (Germany) over the last 40 years and revealed a significant increase in the number of days per month

<sup>1</sup>Institute of Oceanography, University of Hamburg, Hamburg, Germany.

<sup>2</sup>Institute of Geosciences, University of Potsdam, Potsdam, Germany.

<sup>3</sup>Institute of Geophysics, University of Hamburg, Hamburg, Germany.

<sup>4</sup>Institute of Geosciences, University of Bremen, Bremen, Germany.

affected by strong microseisms. The implied increase in wave height in the main source area offshore Norway corresponds with increased surface air temperature and storminess in this region and thus suggests a common forcing.

[4] However, a prerequisite for using microseism data as a proxy for the ocean wave climate is to accurately define the generation areas of microseisms. In a previous study, we used ocean wave models to locate the main source area of microseisms detected at the seismic station in Hamburg [Essen *et al.*, 1999]. The survey clearly suggested that the Norwegian coast is the main source area for microseisms in northern Germany. In this study we further investigate the importance of the Norwegian coast as the source area for microseisms as well as to identify other source areas. Although Grevenmeyer *et al.* [2000] implied a worsening of the ocean wave climate, the observed trend could be related to a shift in the track of weather systems toward the Norwegian coast. However, if other important source areas and seismic stations sensitive to activity in those areas could be detected, microseisms might be a treasure trove for the assessment of the ocean wave climate on decadal scales. Therefore the aim of this study is to further investigate both the generation areas of microseisms and the methodologies to locate them.

[5] Our study uses data from the first European Radar Ocean Sensing (EuroROSE) experiment recorded between 21 February and 26 March 2000. The objective of the EuroROSE project is to develop a radar-based ocean monitoring system in support of safe navigation in port approaches and other densely operated sea areas. In the first experiment, the coastal waters offshore of Norway near 60°N (see Figure 1) were surveyed. Ocean waves were measured by a directional wave rider buoy which yields the spectral distribution of wave height, mean wave direction, and directional spreading. In addition, the microwave radar WAMOS (wave monitoring system) measured the two-dimensional ocean wave height spectrum. These data provide a unique data set to identify a main source area of microseisms. In addition, a numerical forecast model supplies the spatial distribution of ocean waves on a regional scale over the whole North Atlantic. Microseism data from four broadband stations (Kongsberg (KONO) in southern Norway, Bad Segeberg (BSEG) in northern Germany, Gräfenberg (GRFO) in southern Germany, and Eskdalemuir (ESK) in Scotland) and three arrays (NORSAR in southern Norway, GRF in southern Germany, and EKA in Scotland) are investigated (see Figure 1).

## 2. Data

### 2.1. Model Wave Fields

[6] The model ocean wave data were provided by the forecast system of the German Weather Service (DWD). The wave model used (WAM) is one of the best tested models in the world [Komen *et al.*, 1994]. The model describes the development of the two-dimensional wave height spectrum which is discretized in 25 frequency and 24 directional bins. Studying comparisons of wave heights computed by the model and observed by ships, buoys and satellites, Komen *et al.* [1994] concluded that typically, a bias of 10 cm is obtained and a scatter of 20%. The North

Atlantic wave model of the DWD is forced by the wind fields of a global atmospheric model. The wave height includes contributions from wind sea and swell. The data used in this study are the model wave fields calculated on the basis of measured parameters at 0000 and 1200 UTC and the 6-hour forecasts at 0600 and 1800 UTC. The grid point spacing of the model is 1.25° both in latitude and longitude. Our investigations are confined to the area north of 42°N and east of 30°W. Figure 1 shows this area and displays four examples of model wave fields. In addition, Figure 1 shows the positions of the seismic stations under consideration.

### 2.2. Buoy Measurements

[7] A directional waverider buoy was deployed about 8 km off the chain of islands near the Norwegian coast at 60.72°N, 4.60°E (center of gray circle in Figure 1). The directional waverider measures time series of wave height and the horizontal slope vector. With these data, frequency spectra were computed for the wave height, the mean wave direction and the spreading of the azimuthal distribution. The ocean waves can also be characterized by the significant wave height  $h_s$  (the mean height of the highest 1/3 of the waves) and the mean wave direction. Time series of these parameters are displayed in Figure 2. The measurements are compared with model results from the nearest grid point (75 km northwest of the buoy). A correlation coefficient of 0.88 is found between significant wave heights measured by the buoy and determined by the model.

[8] In accordance with the model data, a sampling rate of 6 hours was chosen for the buoy data (which misses the highest significant wave height of 11.5 m on 6 March, 2200 UTC). During the 34-day measuring period,  $h_s$  varied between values of less than 2 m and greater than 11 m. The lowest peak frequency observed was 0.065 Hz which corresponds to an ocean wavelength of 370 m in deep water. The arrows in Figure 2 indicate peaks of the significant wave height which are higher than 5 m. These peaks will be related to the microseism recordings discussed below.

### 2.3. Radar Observations

[9] A common marine X-band radar can be used for sensing ocean wave fields. Information on the wave field is obtained from the radar backscatter from the ocean sea surface (commonly referred to as sea clutter). The German research institute GKSS developed a wave monitoring system, called WAMOS, which samples wave field images. Fourier analysis of a sequence of images yields the two-dimensional wave height spectrum. The signal-to-noise ratio of the images is used for estimating the absolute wave height [Nieto Borge *et al.*, 1999]. Figure 3 displays four two-dimensional wave spectra as measured by WAMOS at the times considered in Figure 1. Three of the wave spectra refer to periods with high waves, i.e., to peak frequency times indicated in Figure 2. These spectra contain waves traveling in the opposite direction to the main wave field, giving rise to the wave-wave interaction needed to generate secondary microseisms [Longuet-Higgins, 1950; Hasselmann, 1963]. Data from an area of 1250 m (north-south)  $\times$  800 m (east-west) within the radar footprint were used to compute the two-dimensional wave spectra. Thus the upper wavelength limit is 400 m. The lower limit is 30 m, determined by the

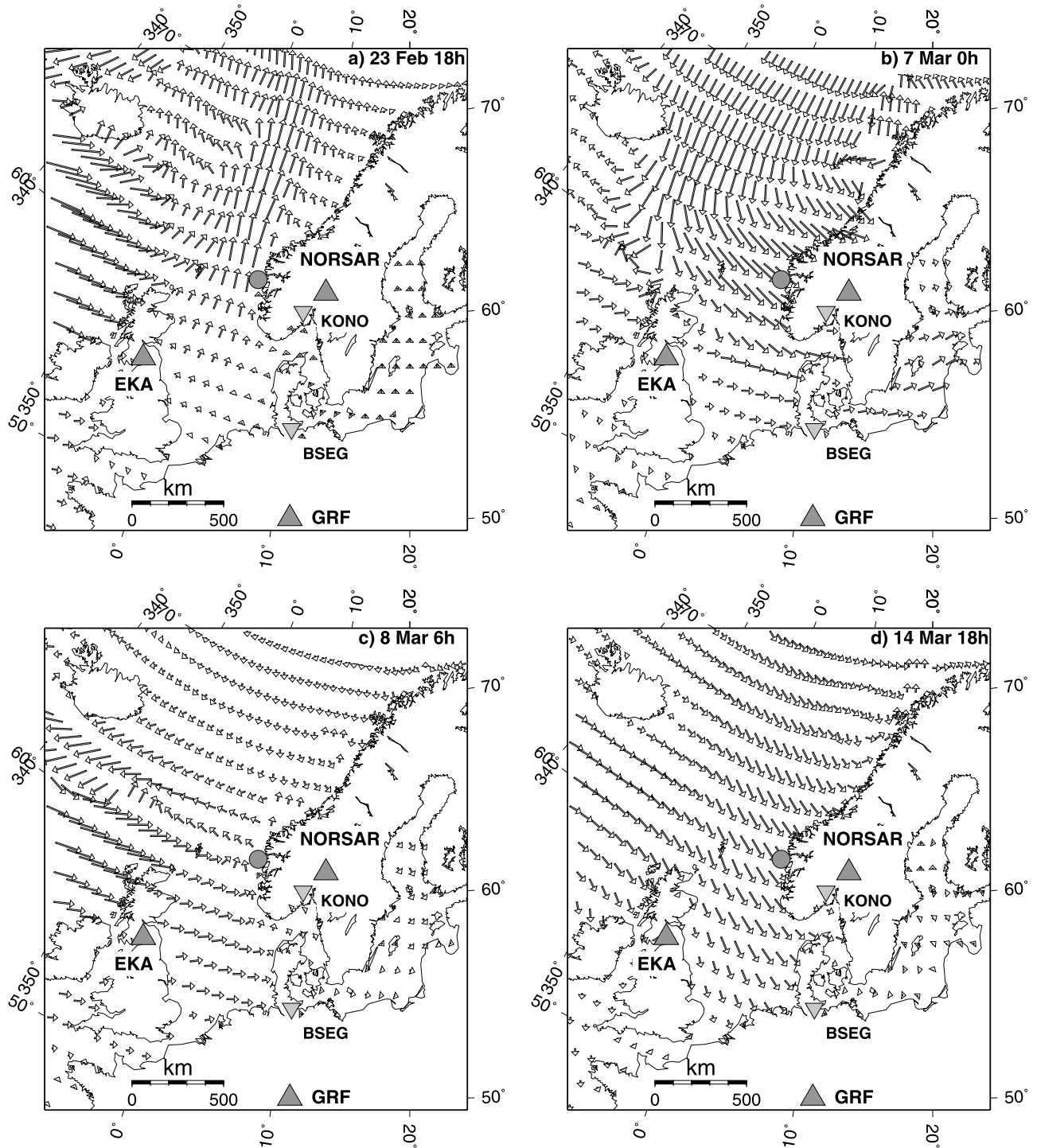


**Figure 1.** Model wave fields. The length of the arrows is proportional to the wave height, composed of swell and wind sea, and the direction points in the direction of wave propagation. The times of the storms are indicated in Figure 2: (a) peak 1, (b) peak 6, (c) diamond, (d) peak 7. The circle at the Norwegian coast indicates the EuroROSE measuring area. Triangles indicate the positions of seismic arrays (NORSAR (south Norway), GRF (southern Germany), EKA (Scotland)) and seismic broadband stations used (KONO (south Norway), BSEG (northern Germany), GRFO (within GRF), ESK (within EKA)). The length scale is set at 49.4°N.

antenna repetition rate. In terms of frequency, the measuring range is 0.06–0.22 Hz.

[10] Table 1 summarizes the parameters of the ocean wave peaks as determined by the model and measured by

the waverider buoy and WAMOS. Comparing measured wave heights reveals some differences, which may be due to limited resolution of the radar (of very long waves) or the different locations of the measurement systems. The

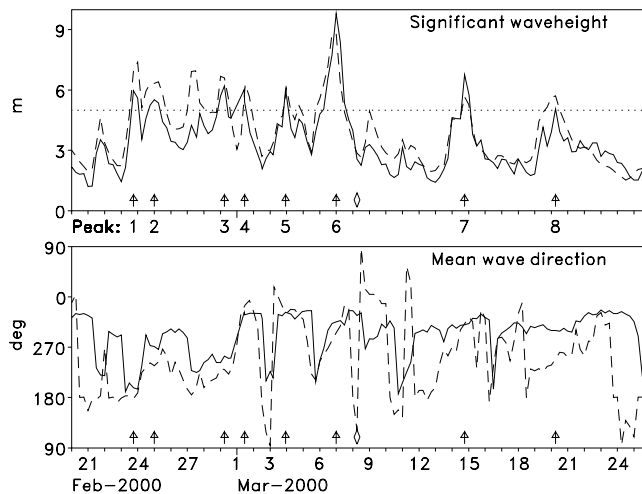


**Figure 2.** Significant wave height and mean direction of ocean waves: buoy measurements at 60.72°N, 4.60°E (solid lines) and model results at 61.25°N, 3.75°E (dashed lines). The eight arrows indicate peak times at which the measured significant wave height exceeds 5 m (horizontal dotted line in Figure 2, top). The diamond indicates the time of the storm at the Scottish coast presented in Figure 1c.

WAMOS is located on a coastal cliff and views the sea surface just in front ( $\approx 2$  km) of the cliff. However, model wave heights and directions agree fairly well with those of the buoy measurements.

#### 2.4. Microseism Data

[11] Data from four seismic stations are investigated. The stations are located in central and northern Europe. BSEG (Bad Segeberg in northern Germany, 53.935°N, 10.317°E) is located in a cave in anhydrite underlain by 5 km of sediments. GRFO (Gräfenberg in southern Germany, 49.691°N, 11.220°E) is located in a 7-inch borehole at a depth of 116 m above 1 km of sediments. In addition, two stations in northern Europe have been chosen, KONO (Kongsberg in southern Norway, 59.6491°N, 9.5982°E) and ESK (Eskdalemuir in Scotland, 55.3167°N, 3.2050°W), both located on hard rock. All the stations are equipped with broadband seismometers. The locations are shown on the maps of Figure 1 together with the positions of three seismic arrays (NORSAR, GRF, EKA). GRFO is located at GRF, and ESK is located at EKA.

[12] Analysis of microseism data was performed in the same manner as of the ocean wave data. The sampling rate is 6 hours. We used 800-s time series (of velocity) sampled at 1 Hz. Spectral smoothing was performed by adding the variance spectra of seven partial 200-s time series with 50% overlap. Fourier spectra of ground velocity were computed with 0.005 Hz resolution, and data sections were weighted by a Hanning window. Thus the 95% error bars on the spectral values are about 6 dB. In accordance with the significant wave height, mean microseism amplitudes were determined by the square root of the total spectral variance of the band 0.1–0.25 Hz. The time series contain little energy below 0.1 Hz. Thus our investigations were restricted to secondary microseisms.

[13] Figure 4 (top) displays an example of an 800-s microseism recording of the vertical component of velocity. Figure 4 (bottom) compares variance spectra of ocean wave height and microseism displacement at the time of the highest sea state during the EuroROSE experiment (event 6). Vertical displacement spectra are displayed; the horizontal components look similar. The coincidence of the peak frequencies (displayed on different scales) suggests that secondary microseisms dominate the recordings. The spectra from the four seismic stations decrease differently with increasing frequency. This behavior may be explained in part by a stronger attenuation of higher frequencies over longer propagation paths.

[14] Figure 5 displays the mean amplitude of displacement at the seismic stations under consideration from 21 February to 26 March 2000. A first comparison of microseism activity with wave activity along the Norwegian coast is given by the eight arrows in Figure 5, which indicate times at which the significant wave height reaches a local maximum. In general, the microseisms show a close similarity to the wave field at the Norwegian coast. However, it is remarkable that there is only minimal microseism response to the ocean wave peaks 1 (23 February), 4 (1 March) and 5 (4 March). On the other hand, there are periods of high microseisms, especially at GRFO and ESK, which presumably did not originate at the Norwegian coast, e.g., the peak on 8 March. This conclusion is supported by the low amplitude of the two-dimensional wave height spectrum shown in Figure 3c.

### 3. Location of Microseism Generation Areas

[15] Two methods are applied to determine the generation areas. First, microseism amplitudes are compared with model ocean wave heights in the North Atlantic Ocean. Areas of maximum correlation are determined. We assume that these areas are generation areas of microseisms in the ocean. Second, an attempt is made to locate generation areas from the azimuthal direction of the microseisms at different locations using array analysis.

#### 3.1. Correlation of Amplitudes

[16] In order to quantify the relation between the ocean wave amplitudes (Figure 2) and microseism amplitudes (Figure 5), correlation coefficients have been calculated. Wave amplitudes are taken from the buoy measurements and the model results at a grid point spacing of 1.25° over the North Atlantic. A similar approach has been used by *Essen et al.* [1999] and by *Bromirski* [2001], who used only buoy measurements. The typical propagation speed of microseism waves is 4 km s<sup>-1</sup>, suggesting that the propagation time from the Norwegian coast to the seismic stations considered is less than 10 min. Both the ocean surface wave field and the microseisms remain stationary over several hours. For this reason, the correlation is performed at zero lag. The correlation coefficients presented are the average for the 34-day study period.

[17] In general, the correlation between ocean wave amplitudes and the square root of the microseism amplitudes is 5% higher than the correlation between the amplitudes. This finding is in accordance with the theory for the generation of secondary microseisms in coastal areas [e.g.,

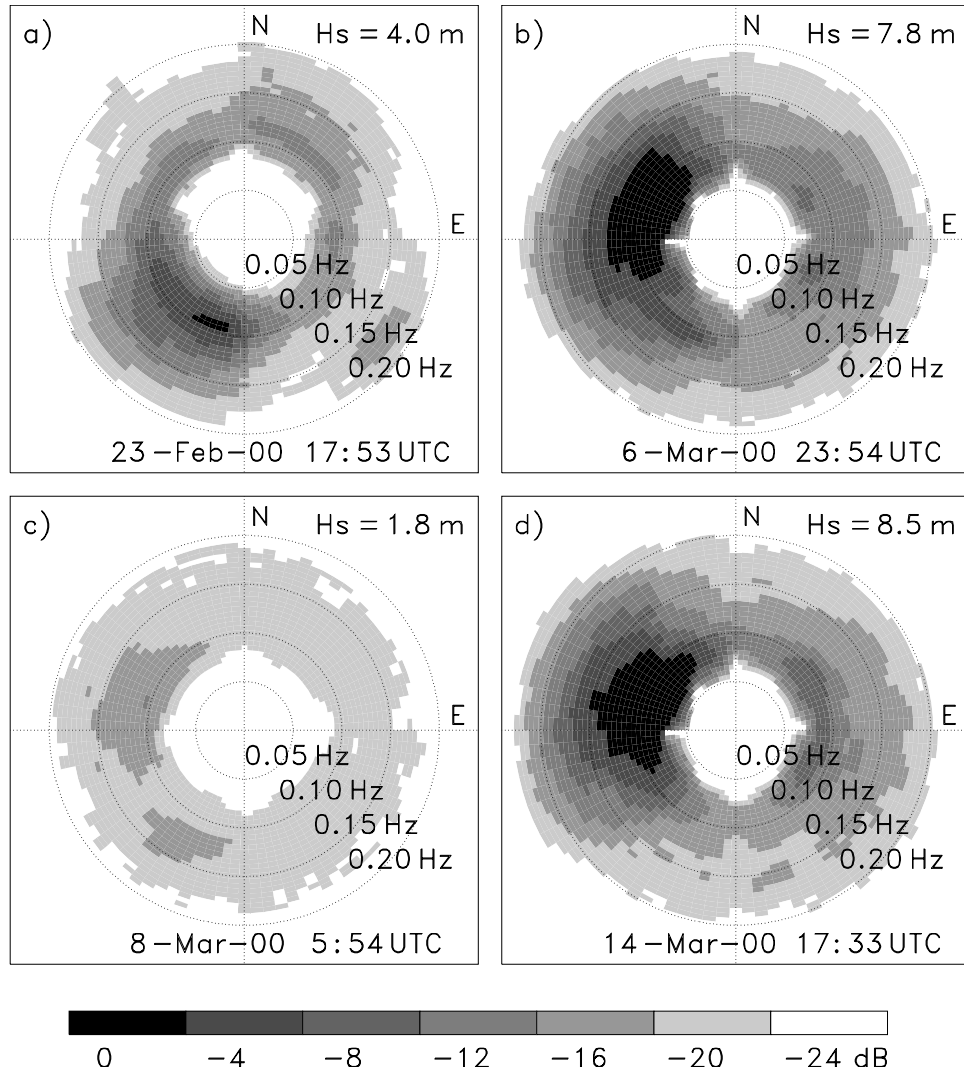


**Figure 3.** Directional frequency spectra of the wave height measured by the radar system WAMOS. Times correspond to those of Figure 1. Black areas describe spectral variances exceeding the maximum value of measurement in Figure 3a.

EsSEN *et al.*, 1999]. Thus we cross-correlate the amplitudes of ocean wave height and the square root of the microseism amplitudes. Considering the vertical microseism component, correlation coefficients with the buoy/model wave amplitudes were 0.78/0.76 at KONO, 0.75/0.72 at BSEG, 0.63/0.61 at GRFO, and 0.36/0.42 at ESK. The model grid point is 75 km northwest of the buoy; see Figure 1. Considering the horizontal microseism component, the correlation coefficients deviate by less than 5%.

[18] The correlation between microseism amplitudes and measured or predicted wave heights agree well. Thus we conclude that we can use the model wave data to estimate the correlation between microseisms and ocean wave heights for each single grid point. Maps of correlation coefficients are presented in Figure 6. Results for the vertical components of the microseism recordings are shown, horizontal components yield almost identical maps. The BSEG recordings yield correlation coefficients above 0.7 (Figure 6b). They are concentrated in a limited area off the south Norwegian coast between 60.0° and 62.5°N which,

by chance, includes the EuroROSE experimental area. The maximum correlation coefficient is 0.73. When considering the GRFO data (Figure 6c), the areas of high correlation are about the same as for BSEG, but the correlation coefficients

**Table 1.** Ocean Wave Parameters<sup>a</sup>

Peak	Date	Time, <sup>b</sup> UTC	$h_s$			$\varphi_m$			$\nu_p$		
			mo	wr	ra	mo	wr	ra	mo	wr	ra
1	23 Feb.	1800	5.8	6.0	4.0	174	197	196	0.083	0.103	0.090
2	25 Feb.	0000	6.0	5.5	5.6	253	271	252	0.086	0.097	0.095
3	29 Feb.	0600	6.8	6.2	6.7	232	254	248	0.100	0.086	0.090
4	1 March	1200	5.6	5.4	5.6	336	328	288	0.097	0.080	0.090
5	4 March	0000	6.7	6.0	5.0	331	333	288	0.103	0.080	0.090
6	7 March	0000	8.1	9.8	7.8	296	316	292	0.113	0.066	0.08
7	14 March	1800	5.7	6.8	8.5	308	310	288	0.095	0.084	0.095
8	20 March	0600	4.8	5.0	5.0	261	300	280	0.062	0.083	0.115

<sup>a</sup>Significant wave height  $h_s$ (m), mean wave direction  $\varphi_m$  (deg), and peak frequency  $\nu_p$  (Hz). Data sources are model (mo) at the closest grid point to the waverider buoy (60.0°N, 3.75°E), waverider (wr) 10 km off coast, and microwave radar WAMOS (ra) 2 km off coast.

<sup>b</sup>Times are those indicated by arrows in Figure 2.

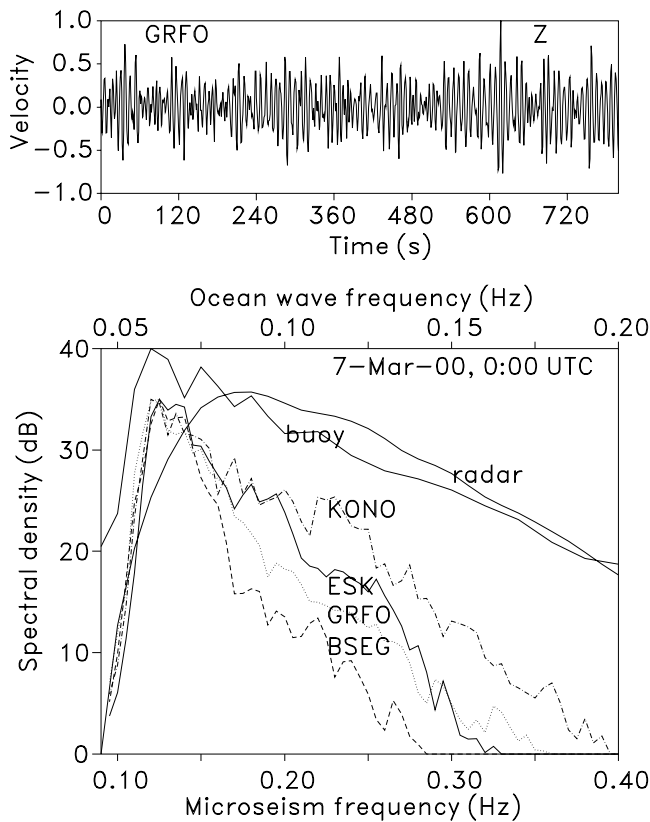


**Figure 4.** (top) Example of a microseism data recorded at GRFO (7 March, 0000, wave height peak event 6). (bottom) Comparison of ocean wave height spectra measured by buoy and radar with microseism spectra of the vertical displacement at the seismic stations KONO, BSEG, GRFO, and ESK (event 6). The normalization of the two ocean wave spectra (solid lines) is common; the normalization of the microseism spectra is arbitrary. The frequency scales of ocean waves and microseisms show the expected 1-to-2 relation.

are smaller by about 0.05, i.e., by 7%. Off the Scottish coast, the GRFO correlation coefficients (maximum 0.67) are higher than the BSEG ones (maximum 0.62).

[19] The correlation map of KONO (Figure 6a) is very similar to that of BSEG. The maximum correlation coefficient is 0.78 at 60°N. An additional area with correlation coefficients higher than 0.7 is located in the Skagerrak (around 58°N, 8°E), just south of the recording station. The correlation map of ESK (Figure 6d) reveals low values at the south Norwegian coast and higher values around Scotland, where the recording station is located. There is a small area at the Atlantic coast with a correlation coefficient of 0.71, i.e., higher than 0.7.

**3.2. Location With Seismic Arrays**

[20] Numerous investigations using array data have contributed to the understanding of the generation of microseisms. The microseism noise situation around Norway was studied by Bungum *et al.* [1971, 1985] and by Friedrich *et al.* [1998] among others. Seismic arrays enable the direct estimation of the direction of incoming wave fields [Harjes and Henger, 1973]. Secondary oceanic microseisms are

supposed to consist mainly of Rayleigh wave fundamental modes [Hasselmann, 1963]. Because of their nature as surface waves only the back azimuth of the incoming wave field can be determined with a seismic array. That means that several arrays around the possible generation areas for microseism waves are needed to constrain a specific area [Cessaro and Chan, 1989; Cessaro, 1994; Friedrich *et al.*, 1998]. We used three arrays in Norway (NORSAR), Germany (GRF), and Scotland (EKA) to analyze the wave field characteristics on 6 March 2000, 2300, to 7 March, 0000 (highest wave height at the buoy) and on 8 March 2000, 0600–0700 (highest waves north of Scotland).

[21] The GRF array is located in southeast Germany and consists of 13 broadband (vertical) Streckeisen STS1 sensors (sampling rate 20 Hz). The array is L-shaped with a maximum aperture in the N-S direction of about 100 km and an E-W aperture of about 50 km. The array is located on jurassic limestone underlain by older sediments. The NORSAR array is located in southeast Norway and has 6 broadband three-component stations and 26 short-period stations with an average aperture of about 70 km. Compared to the above arrays, the short-period EKA detection array (colocated with the broadband station ESK in Scotland) is of smaller aperture (20 short period vertical sensors

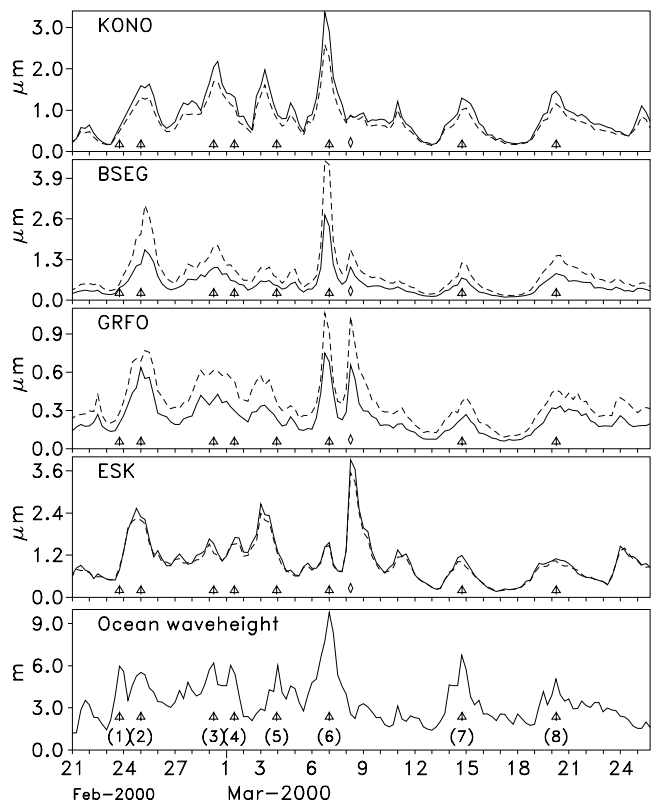


**Figure 5.** Mean microseism displacement amplitudes at four seismic stations: vertical component (solid line), vector amplitude determined from the two orthogonal horizontal components (dashed line). The sampling rate is 6 hours. The ocean wave height of Figure 2 is displayed for comparison. The arrows indicate times of maximum significant wave height at the EuroROSE area; see Figure 2. The diamond indicates the time of the storm at the Scottish coast presented in Figure 1c.

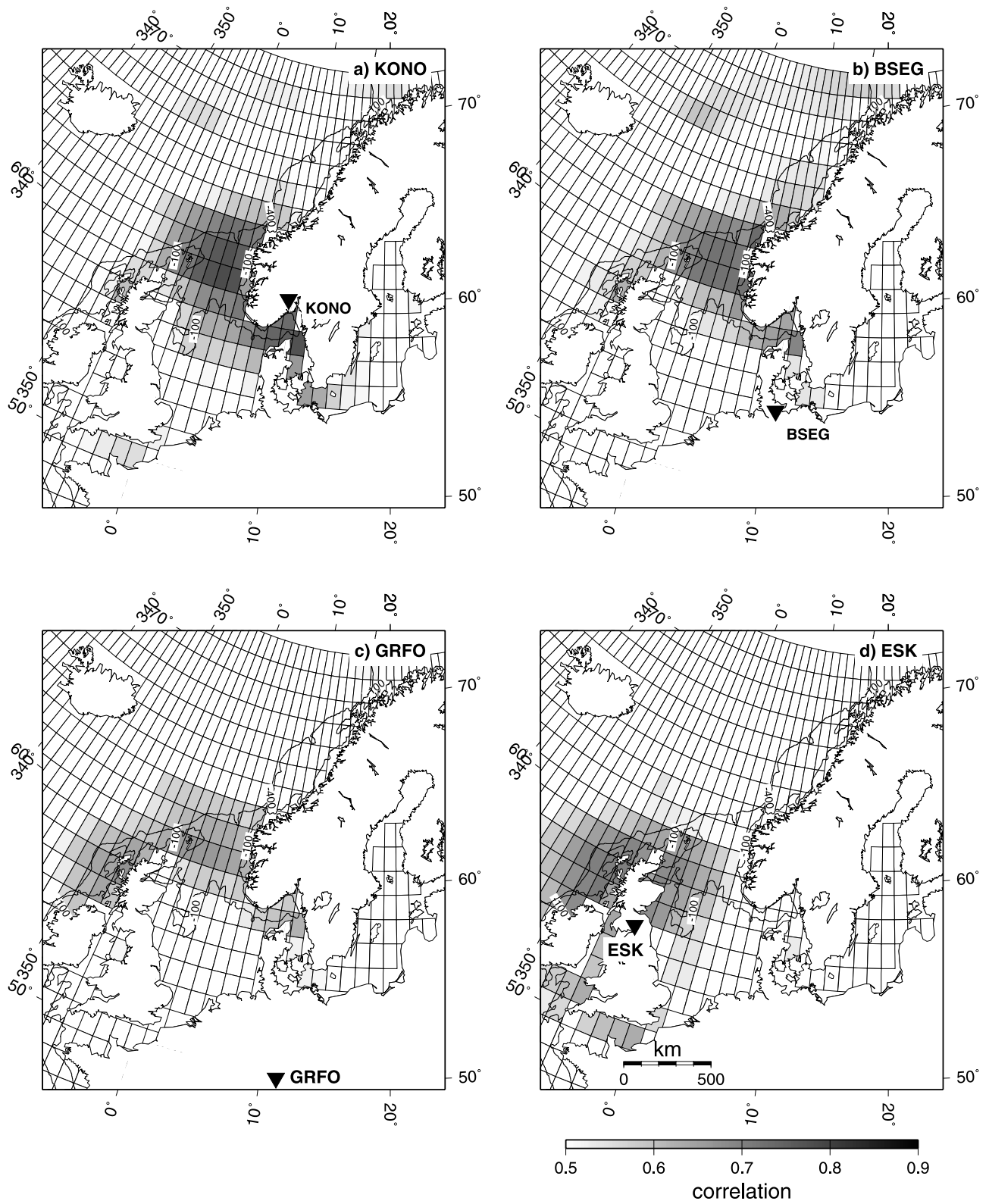


**Figure 6.** Maps of the correlation between model ocean wave amplitudes and root amplitudes of the vertical microseism displacement recorded at KONO, BSEG, GRFO, and ESK. Locations of the seismic stations are shown. The 100 and 400 m depth contours are displayed. The length scale is set at 49.4°N.

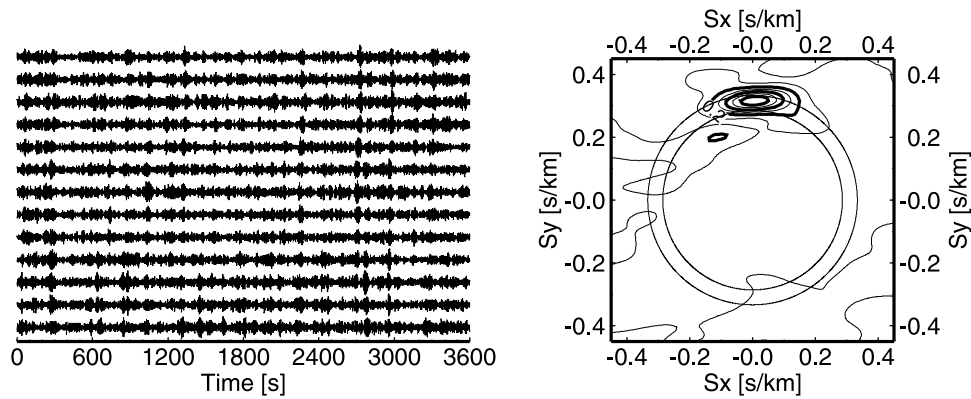


**Figure 7.** (left) Example of the seismograms recorded at the GRF array on 6 March 2000, 2300. (right) The corresponding semblance map in slowness domain. The velocity window of  $3.0\text{--}3.5\text{ km s}^{-1}$  is indicated by the two circles.

arranged in an L) of only about 8 km and therefore has poorer direction resolution capability.

[22] For the direction estimation the frequency-wave number analysis technique was used [Kvaerna and Ringdahl, 1986]. The routine used performs a grid search over a Cartesian slowness grid ranging from  $-0.5$  to  $+0.5\text{ s km}^{-1}$  with  $0.01\text{ s km}^{-1}$  grid interval in  $x$  and  $y$  direction in a frequency range from  $0.1$  to  $0.2\text{ Hz}$ . One hour of data was analyzed, ensuring averaging of about 360 samples in the frequency domain. The use of a frequency band below the corner frequency of short-period sensors (NORSAR, EKA) was tested and posed no problem.

[23] Figure 7 shows as an example the seismograms recorded at the GRF array starting at 6 March, 2300, and the corresponding semblance map in slowness domain. The resulting maps of the semblance, i.e., the ratio of the averaged power of the stacked trace and the stack of the averaged single trace powers, which defines a measure of coherency [Neidell and Taner, 1971], usually show one or more maxima at slownesses corresponding to horizontal velocities typical for the fundamental Rayleigh mode at the respective dominant periods ( $3.0\text{--}3.5\text{ km s}^{-1}$ ).

[24] It is well known that surface waves suffer scattering and refraction on their way from the source region to the receivers [Friedrich et al., 1994] leading to deviations of the apparent direction of approach compared to the true great circle direction. To check for any systematic bias of the direction estimates, we processed the Rayleigh waves of several earthquakes in Northern Europe (small solid circles in Figure 8) in the same frequency band as the microseisms. This “array calibration” procedure is a standard technique for detection arrays and body waves [Koch and Kradolfer, 1999]. The direction deviation problem is especially relevant for the GRF array, which is the most distant with respect to the probable generation areas. Events in the distance range up to  $7^\circ$  show back azimuth deviations smaller than about  $5^\circ$ , which is about the resolution limit of GRF (Figure 7). Events farther away from northwesterly directions show a systematic shift to northern directions. Especially interesting are three events which were located not very far from the buoy position (Figure 8). Their average direction deviation at GRF is  $+13^\circ$ . For one event not far from the buoy position, a deviation of about  $-5^\circ$  is

found for EKA and about  $-1^\circ$  for NORSAR. Generally, direction deviations at NORSAR are small ( $\leq 7^\circ$ ).

[25] Figure 8a shows the array direction estimation results for 6 March, 2300, to 7 March, 0000, and Figure 8b shows the results for 8 March, 0600–0700. In Figure 8 (bottom) the array semblance values as functions of back azimuth are shown. Only the semblance values in the horizontal velocity window corresponding to Rayleigh wave fundamental modes ( $3.0\text{--}3.5\text{ km s}^{-1}$ ) were used. The width of the main peaks is representative for the resolution and is directly proportional to the array aperture. The “rays” in Figure 8 show the corresponding directions projected onto a map of the area (ray width and gray shading is proportional to the semblance).

[26] For the storm on 6/7 March (midnight) the GRF and the NORSAR array both point toward the southwest Norwegian coast slightly north of the buoy position (see Figure 8a). The crossing point of both back azimuthal ‘rays’ is located at  $61.75^\circ\text{N}$ ,  $5.51^\circ\text{E}$  using a spherical earth approximation (Figure 8). Here we applied an azimuthal correction factor of  $-13^\circ$  to the GRF “raw” result. For the NORSAR array no direction correction needs to be applied because it is located close to the source area (and is of large aperture). EKA shows a broad beam pattern pointing northward. Applying the azimuthal correction for the event near the buoy shifts the estimated direction somewhat westward (by  $+5^\circ$ ). We interpret this situation to be caused by superposed wave fields originating near southwest Norway and the Scottish coast at the same time, which cannot be discriminated because of the low resolution of EKA.

[27] On the morning of 8 March, ocean waves were high north of Scotland and low off the Norwegian coast. Accordingly, the azimuthal directions observed at GRF and EKA both point toward the northwest Scottish and Irish coasts. The semblance at GRF (see Figure 8b, bottom) is considerably smaller than for the previous example, reflecting either a larger extent of the source area, more complex crustal structure along the propagation path and/or the arrival of microseisms from other source areas. The situation at NORSAR is more complex. The largest peak points toward north-northwest and corresponds to a local generation area. A second broader peak

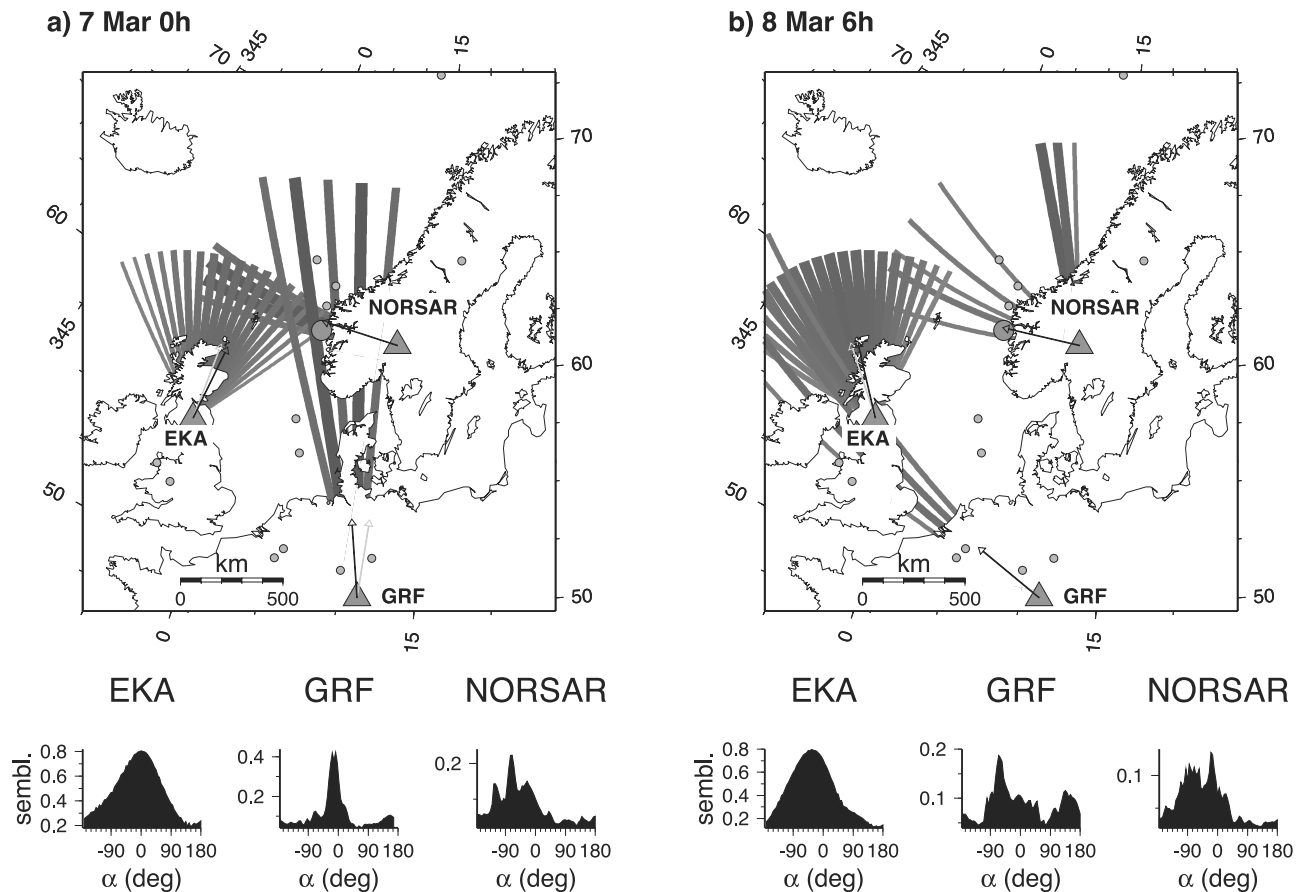


**Figure 8.** Array beam directions of the incoming wave field for (a) 7 March, 0000, and (b) 8 March, 0600. (bottom) Diagrams of the semblance (coherency in the frequency band 0.1–0.2 Hz for 1 hour of data) as a function of back azimuth for a velocity window of 3.0–3.5 km s<sup>-1</sup> (Rayleigh waves fundamental modes). The semblance as function of back azimuth is shown as beam directions with varying gray scales and line widths on a map in the upper panels, where a cutoff coherency has been defined at about 30% of the individual semblance range. The arrows show the directions of the semblance before (gray) and after the angle deviation correction. Small solid circles indicate locations of earthquakes that have been used to calibrate the angular deviation at the arrays. The length scale is set at 49.4°N.

points toward the west. The corresponding ray pattern does not intersect with those of the other two arrays at the coastal areas of northwest Scotland (and Ireland), but points more into the open ocean between Scotland and Ireland. This “deviating” result is probably produced by refraction and scattering of the corresponding wave trains through geological structures in the North Sea. In this region we did not have recordings of sufficiently strong earthquakes to check for azimuthal deviations. Applying the corrections of about  $-4^\circ$  (GRF) and  $-5^\circ$  (NORSAR) found from two earthquakes in southwestern England (see Figure 8) to the GRF and NORSAR results would move the array beams only slightly closer together.

[28] The array beam patterns at NORSAR (not shown here) for the other days with high ocean wave fields at the buoy position (Table 1) show about the same characteristic as for the days discussed above, with broad beam patterns and predominance of semblance peaks shifting to the north or south within a back azimuth range from about  $-110^\circ$  to about  $+10^\circ$ . With the exception of 23 February (low microseism amplitudes), the GRF beam pattern maxima

point toward north (Norway); for EKA the north/northwest directions are always illuminated.

## 4. Discussion

### 4.1. Generation Areas

[29] Land-based seismometer studies on generation areas of microseisms give conflicting results. *Darbyshire* [1991] and *Cessaro* [1994] located secondary microseisms arriving from the open ocean that appear to be generated beneath storms in the deep sea as well as near the coast. In contrast, *Haubrich and McCamy* [1969] did not observe significant amounts of energy from the open ocean, suggesting that microseism energy is generated near the coast. However, *Gutenberg* [1947] was able to trace a hurricane traveling through the Caribbean Sea, far from the shore. *Bromirski* [2001] also investigated this issue using land-based seismometers and buoys located offshore the U.S. east coast during the famous October 1991 “Perfect Storm.” He suggested that the extreme wave conditions occurring during this storm, in conjunction with the occurrence of Hurricane

Grace to the south, are ideal for studying where secondary microseisms originate. Bromirski [2001] concluded that the dominant source area for secondary microseisms is near the coast and not in the open ocean. The same conclusion was reached by Bromirski and Duennebier [2002].

[30] The Norwegian coast was reported to be the main source area of microseisms recorded on seismic stations in northern Europe and even in Russia [Gutenberg, 1921; Bath, 1949; Strobach, 1962; Darbyshire, 1992]. In our approach we tried to define regions in Europe affected by waves approaching Norway. In addition, we tried to define major source areas for northern Europe. We utilized digital data analysis of both waves and microseisms. This is an important improvement compared to most previous studies carried out in Europe. A significant advantage of digital data analyses is the power of spectral and statistic investigation of time series, which allow a formal correlation of microseisms and wave data from both measurements and wave models. Early studies of microseisms were generally based on the coincidence between the sea state, storms in coastal areas, and strong seismic signals with periods of 4–16 s recorded on seismographs, often hundreds of kilometers away from the coasts.

[31] Different source areas will always be difficult to define because large weather systems which generate ocean waves generally impact different shore lines and hence provide multiple concurrent source areas for microseisms. For example, on 14 March all the seismological stations indicate strong microseisms (Figure 5). Figure 1 shows the wave field on the western European coast lines. Strong waves approach the coasts of both Norway and the British Isles. Another potential generation area for microseisms is the Gulf of Biscay [Gutenberg, 1921; Strobach, 1962; Friedrich et al., 1998]. However, during the storms generating microseisms discussed here, the sea there was relatively calm. Therefore we suggest that the major generation areas recorded by the stations surveyed during the time span studied are most likely the British and Norwegian coasts. To define these source areas, we used the microseism time series and the model ocean wave data and calculated the correlation coefficients for each grid point from the 34-day time series (Figure 6). High correlation coefficients are interpreted as indicating a close relationship between wave activity and microseisms, thus indicating generation areas. This approach establishes that Norway and northern Germany are primarily affected by wave activity off southwest Norway. Also, southern Germany is affected by microseisms from southwest Norway. In addition, southern Germany is affected by microseism energy generated at the coast of Scotland, which were not so prominently recorded in northern Germany and Norway. However, for Scotland the most important source area of microseisms seems to be its own coast lines.

[32] The highest correlation was obtained between ocean wave amplitudes in southwest Norway and the microseism amplitudes in northern Germany (BSEG) and southwest Norway (KONO). Correlation coefficients exceed 0.7. Even microseisms in southern Germany (GRFO) show a close relationship with the buoy data, although the correlation is lower ( $\approx 0.6$ ). Although ESK in Scotland is much closer to the study area than GRFO in southern Germany, it shows a very low correlation of less than 0.4. However, we have to

keep in mind that the correlation analysis favors the most prominent peaks and not the absolute amplitude of ground motion. For example, on 7 March (peak 6) KONO, BSEG, and GRFO show a prominent peak while the same peak is less dominant at ESK (Figure 5). Compared to GRFO, the station ESK is much closer to the source area off Norway and hence recorded a larger displacement than GRFO. The same phenomenon is observed on the following day (8 March). Here, ESK recorded a very strong microseism storm and GRFO also indicates a very prominent peak of microseisms. The peak was not detected by KONO and was very weak at BSEG. In terms of absolute amplitude, the event generated a larger displacement at BSEG than at GRFO. This is, of course, related to the spreading of seismic energy, which is a function of distance from the source area. In addition, it is important to note that the event on 8 March is not related to any wave activity off southern Norway, hence suggesting a second generation area near or at the Scottish coast.

[33] The seismic array analysis also clearly reveals the southwest Norwegian coast as the dominant source area on 6/7 March, while the Scottish and Irish coastlines are active on 8 March (Figure 8). The array results also show that (except for the most inland GRF array) the local coastline always contributes to the (locally) observed wave field and is sometimes the dominant component. Our data favor the coastlines as the major generation areas, but because of the resolution limits of the array data, we can not rule out the possibility that parts of the microseism wave field are generated in the open ocean (see the ocean wave field and the directions for 8 March). This result is in agreement with the correlation analysis, which also shows the highest correlation coefficients near the coast. However, this technique has similar limitations. For example, if near the coast and within the adjacent ocean the same wave conditions exist, the correlation would be the same for both areas, even if the interaction between waves and coast generates microseisms.

[34] Taken together, correlation analysis and energy back tracking allow us to locate the dominant source areas. The correlation technique indicates the dominant generation areas over the time period studied. Ocean model wave field data and continuous seismic data from stand-alone stations are needed. However, the correlation method has no temporal resolution, and the spatial resolution is limited. Additionally, correlation is an indirect measure, and thus the generation areas of microseisms may have a smaller extent than the regions showing high correlation coefficients. In contrast, the array analysis is a direct measure of the direction of microseismic generation areas. It has the potential to resolve the spatiotemporal extent of generation areas during single storms, as long as more than two arrays with a sufficient resolving power can be used. The drawback of the array technique is the large amount of seismic data, the computational needs of the processing technique and the array calibration needed. A further increase of the resolving power could probably be reached by fully modeling the seismic wave field in a three-dimensional earth.

#### 4.2. Generation Mechanism and Extent of Coastal Generation Areas

[35] Hasselmann [1963] investigated the theory of the response of a layered elastic half-space to a random homogeneous and stationary pressure field. Appreciable micro-

seisms are generated only by Fourier components of the exciting random field that have the same phase velocities as free modes of the elastic system. The system response consists of trapped Rayleigh modes. A pressure wave on the ocean floor of high phase velocity can be excited by quadratic interaction of ocean surface waves if there are two surface waves of similar frequency traveling in nearly opposite directions so that the difference in wave number is small. The frequency of the pressure wave, and in turn that of the excited elastic wave, is equal to the sum of the two surface waves and hence equal to nearly twice the frequency of the surface wave.

[36] Doubling of microseism peak frequencies has previously been observed [e.g., *Kibblewhite and Ewans, 1985; Sutton and Barstow, 1996; Bromirski, 2001*], and has been interpreted as evidence of nonlinear wave-wave interaction as a generation mechanism. *Babcock et al. [1994]* were able to demonstrate that the double-frequency microseism peak can contain local as well as teleseismic components generated at different locations.

[37] The correlation between the microseism peak frequency at KONO and the double frequency of the ocean wave peak measured at the buoy off the coast of southwest Norway is high (Figure 9). The peak frequency is the weighted mean over a narrow band around the frequency of the maximum spectral variance. This correlation confirms, again, the nonlinear wave-wave interaction as the primary generation mechanism. It is also an indication that most of the microseism energy at KONO is generated by the ocean wave field off the coast of Norway, similar to conclusions drawn before. Although not shown here, the correlation of peak frequencies for the other seismic stations is smaller. During storms, the microseism peak frequencies are about the same at all four stations (Table 2) and about double the ocean wave peak frequencies (see Table 1). The exceptions from this rule may be explained by contributions of microseisms from additional generation areas.

[38] Typically, seismic spectral peaks at higher frequencies ( $>0.2$  Hz) are associated with more local storms and

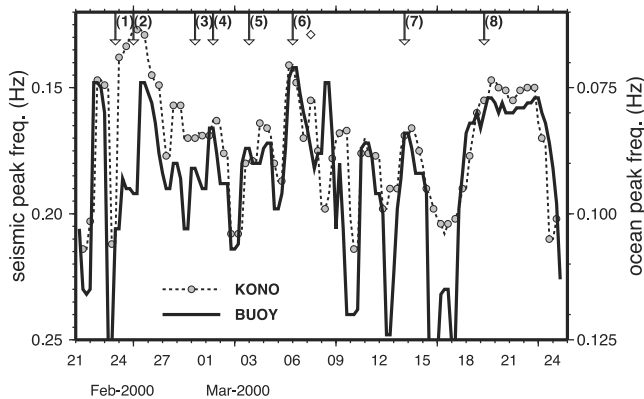


**Figure 9.** Peak frequencies of microseisms at KONO ( $Z$ ) and of the ocean waves as measured by the buoy. The sampling rate is 6 hours, and the data have been slightly smoothed (median filter, three sample points). The arrows indicate times of maximum measured significant wave height; see Figure 2. The diamond indicates the time of the storm at the Scottish coast presented in Figure 1c.

**Table 2.** Microseism Peak Frequencies  $\nu$  and Ratios of Generation Areas  $q^a$

Peak	$\nu_{\text{KONO}}$	$\nu_{\text{BSEG}}$	$\nu_{\text{GRFO}}$	$\nu_{\text{ESK}}$	$q_{\text{KONO}}$	$q_{\text{BSEG}}$	$q_{\text{GRFO}}$	$q_{\text{ESK}}$
1	0.22 <sup>b</sup>	0.16	0.16	0.15	0.9 <sup>b</sup>	1.6	2.1	3.1
2	0.13	0.13	0.13	0.15	0.8	0.8	1.2	1.7
3	0.17	0.16	0.16	0.16	1.1	1.3	1.5	1.8
4	0.15	0.16	0.16	0.16	1.4	1.7	2.1	3.2
5	0.18	0.16	0.17	0.17	1.2	1.7	2.2	3.7
6	0.13	0.13	0.13	0.13	1.0	1.0	1.0	1.0
7	0.17	0.15	0.15	0.15	0.5	0.6	0.6	0.9
8	0.15	0.14	0.15	0.15	1.3	1.2	1.4	1.5

<sup>a</sup>See equation (1), at KONO, BSEG, GRFO, and ESK. Times are those of Table 1 which coincide with the wave height maxima in Figure 2;  $\nu$  unit is Hz; and  $q = \sqrt{A_j/A_6}$  ( $j = 1, \dots, 8$ ).

<sup>b</sup>Seismic measurements made at 1430 since KONO did not record at 1800.

short-period ocean waves, while low frequency microseisms ( $<0.15$  Hz) originate from the long-period swell produced by the larger storms with a center more distant from the coast. The largest microseism amplitudes have been measured during the storm on 6/7 March (peak 6). Peak 6 is also associated with the lowest peak frequency, near 0.14 Hz (Figure 9), indicating that long-period swell arrived at the southwest Norwegian coast. The swell from 6/7 March affected the entire west coast of Norway (Figure 1).

[39] From the correlation maps (Figure 6) we conclude that the southwest Norwegian coast is an important generation area for microseisms recorded in central and northern Europe. However, the areas of high correlation need not correspond to the extent of the generation area. By correlating the wave amplitudes at the grid point near the wave buoy (Figure 2) with the wave amplitudes at the other grid points, about the same correlation peak widths are found as in Figure 6 (about 700–1000 km if the area is used where the correlation coefficient is higher than 0.5). Thus the generation areas of microseisms may be smaller than indicated by Figure 6. From the width of the array beam patterns (Figure 8) we estimate that the extension of the source area in north-south direction is about 500 km (following the Norwegian coastline and well constrained by the NORSAR array) and is not more than 500 km in the east-west direction (constrained by GRF; it is possibly smaller in the east-west direction).

[40] In the following, we try to estimate the extent of the generation areas at the Norwegian coast during the 6/7 March storm and other storms by using the two-dimensional oceanic wave field as measured by the radar system. This system provides independent and new data, and thus a unique chance for such an estimate.

[41] *Hasselmann [1963]* derived a relationship between the one-dimensional variance spectrum  $F$  (power spectrum) of the secondary microseism displacement and the two-dimensional variance spectrum  $f$  of ocean wave height,

$$F(\nu) = \frac{AI(\nu)}{R} \sum_{n=1}^N T_n(\nu) = AI(\nu)T(\nu) \quad (1)$$

$$I(\nu) = \int_0^\pi f\left(\frac{\nu}{2}, \varphi\right) f\left(\frac{\nu}{2}, \varphi + \pi\right) d\varphi,$$

where  $\nu$  is the frequency and  $\varphi$  the direction of the ocean wave component.  $A$  is the extent of the generation area and

$R$  the distance from this area to the receiver. The transfer function  $T(\nu) = (1/R) \sum_{n=1}^N T_n(\nu)$  is different for vertical and horizontal displacements and is a function of frequency  $\nu$  and mode number  $n$ . The total number  $N$  of guided modes depends on the structure of the Earth's crust. Both spectra in equation (1),  $F$  and  $I$ , can be measured at the seismic station and at the footprint of the radar, respectively. This gives the opportunity to directly estimate  $A$ . Previous studies have been based on model spectra of the ocean wave height [Webb, 1992] and assumptions on the reflection coefficients and thus  $I(\nu)$  [Szelwis, 1982].

[42] The reflected energy of waves traveling in opposite direction to the peak energy is found to be about 5% at the radar footprint. This value measured by the radar is in good agreement with theoretically estimated reflection coefficients at the Norwegian coast [Darbyshire, 1992].

[43] The transfer function  $T(\nu)$  depends on the seismic structure between the source area and the receiving station, which is inhomogeneous and uncertain. Therefore we have not tried to calculate absolute transfer functions. The ratio,

$$\gamma(\nu) = F(\nu)/I(\nu), \quad (2)$$

depends on the product  $AT(\nu)$ . Since  $T(\nu)$  is time-independent and  $A$  is independent of frequency  $\nu$ , a variation of  $\gamma$  with  $\nu$  indicates the frequency dependence of  $T(\nu)$ . Using  $F(\nu)$  at KONO and comparing  $\gamma$  for the time of different wave height peaks (see Figure 10) permits studying the variability of the generation area  $A$ .

[44] Figure 10 also compares the wave height spectra measured by the buoy and by the radar. There is a good agreement for frequencies higher than 0.16 Hz (i.e., 0.08 Hz ocean wave frequency). However, long-wave energy is strongly underestimated by the radar (wave height peaks 2, 6, and 8). The ocean wave spectra measured by the buoy and the radar deviate at frequencies below about 0.08 Hz (i.e., wavelengths longer than about 244 m in deep water) which corresponds to microseism frequencies less than 0.16 Hz. This deviation is caused by the limited measuring range of the radar system (0.06–0.22 Hz, see section 2.3). Unfortunately, this means that for some of the wave height peaks (peaks 2, 6, and 8) we cannot compare the measured wave-wave interaction integral with the observed seismic data for the peak values.

[45] In Figure 10, above 0.16 Hz, the spectral ratio  $\gamma$  is relatively flat and of similar shape for most peaks, i.e., there is no distinct frequency dependence of  $T(\nu)$ . The mean high-frequency level of  $\gamma$  varies between  $-24$  and  $-16$  dB, corresponding to a factor of 0.5 (peak 7) to 1.4 (peak 4) of the linear extent (diameter) of the generation area relative to that of peak 6. Table 2 presents these ratios ( $q = \sqrt{A_j/A_6}$  ( $j = 1, \dots, 8$ ); see equation (1)) for the four seismic broadband stations used. There is a good agreement between BSEG and KONO. GRFO and ESK reveal somewhat higher values, which we explain as including contributions from microseisms from source areas other than the southwest Norwegian coast.

[46] In summary, the variability of the extent of the generation area is in general small. This may indicate that  $A$  is controlled by static features such as coastlines or bathymetry, and not by the spatial extent of storms. Peak 6 shows the largest microseism amplitudes, but an average

generation area. From this we conclude that the microseism energy is mainly controlled by the wave height.

[47] In the discussion above we have assumed that the local wave-wave interaction integral measured by the radar system is representative for the whole generation area. This assumption of stationarity of the wave field is justified by the comparison of the buoy and radar system wave height spectra (Figure 10), which shows that for the 6 km apart buoy and radar system locations (Figure 11), the measured wave height spectra are in good agreement for frequencies above 0.16 Hz. Figure 11 indicates that the bathymetry shows a rather steep slope at the coast but is simple and plane in the ocean with depths between 300 m up to about 350 m in a distance of about 5 km from the coastline. This is also favoring stationarity of the wave-wave interaction integral. The small relative angle between the mean wave direction  $\varphi_m$  and the coast line for wave height peak 1 (23 February 1800) can explain the low microseism amplitudes observed at the seismic stations but cannot explain the small ratio  $q$  for wave height peak 7 (14 March, 1800, Table 2).

[48] These complications show that the model (1) is still very simple and cannot account for all effects observed. However, we believe that the conclusion that the size of the generation areas are relatively constant and linked to geographic regions near the coast is justified based on the data we have analyzed.

[49] If one changes the viewpoint and interprets the mismatch between the spectral microseism ratios and the spectral wave-wave interaction integral ratios as being completely due to the imperfect knowledge of the true regional  $I(\nu)$ , a factor of uncertainty of at most 2.8 results for KONO and 2.83 for BSEG, respectively (Table 2), if all peak wave height events are evaluated in common. The “uncertainty” factors for GRFO and ESK are 3.7 and 4.1 (most likely higher due to contributions from other generation areas). The  $q$  ratio being in error by a factor of 2.8 leads on average to a mismatch of about  $\pm 35\%$ , if relative ocean wave heights are estimated from the microseismic data (ocean wave heights being proportional to the 4th root of  $F(\nu)$ ). Longer time series have to be evaluated to substantiate this result, which is important for the accuracy with which historic microseismic recordings can be used to reconstruct the wave climate near the southwestern coast of Norway.

## 5. Conclusions

[50] Ocean wave measurements at the Norwegian coast ( $\approx 60^\circ\text{N}$ ) and model wave data of the North Atlantic Ocean for a period of 34 days in early 2000 are compared to microseism recordings at four land sites in central and northern Europe. The objectives of the microseism investigations were to locate the generation areas and to estimate their spatial extents. Two methods were applied; the computation of correlation maps between microseisms and ocean wave height determined by a wave model, and the location of generating areas by using seismic arrays. In addition, two-dimensional wave height spectra, measured by a radar system, are used to estimate the relative extent of the generation areas during different storms.

[51] High correlations are found between time series of microseism amplitudes recorded in southern Norway

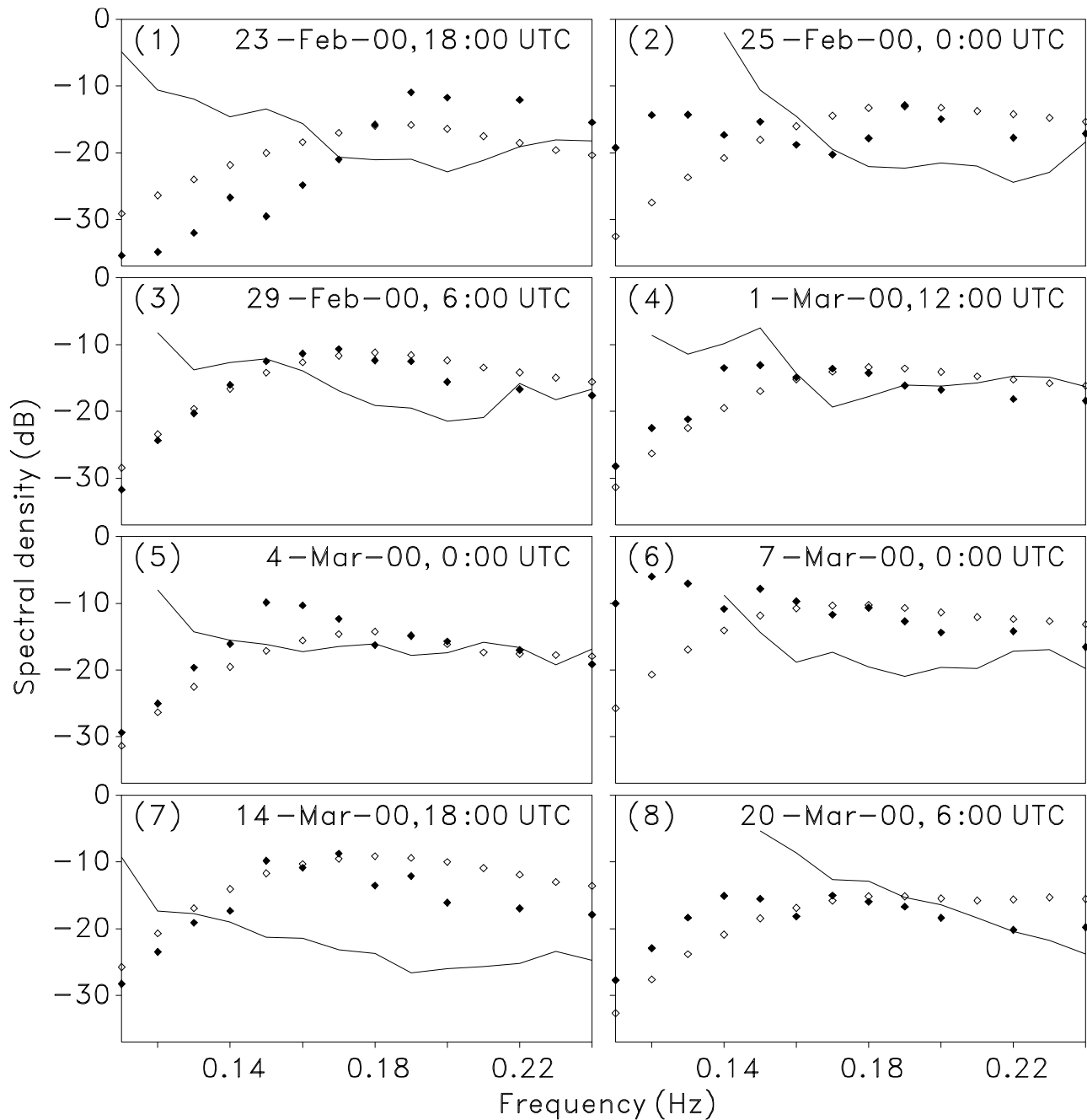


**Figure 10.** Spectral ratio  $\gamma(\nu)$  (solid lines), as defined by equation (2), during eight storms; see Figure 2. For comparison, the wave height spectra measured by the buoy (solid diamonds) and by the radar (open diamonds) are plotted at a doubled frequency scale. All data have a common spectral density scale. For peak 1 the seismic measurements were made at 23 February, 1430, because KONO did not record at 23 February, 1800.

(Kongsberg) and northern Germany (Bad Segeberg) and the significant ocean wave height measured off the southwest Norwegian coast; these are 0.80 and 0.73, respectively (Figure 5). Recordings in southern Germany (Gräfenberg) reveal a somewhat lower correlation of 0.63, and those in Scotland (Eskdalemuir) yield the relatively low value of 0.29. Maps of the correlation between microseisms and model wave fields of the North Atlantic Ocean confirm this finding (Figure 6). Areas of maximum correlation are assumed to be

the main microseism generation areas. For Kongsberg and Bad Segeberg, this area is the Norwegian coast at about  $60^\circ$  (i.e., the wave measuring area). For ESK maximum correlations are found for the model wave fields off the northwest and northeast Scottish coasts. Gräfenberg receives important microseism contributions from this area but also from the British coasts, which are the main generation area for microseisms recorded in Eskdalemuir. These results are in good agreement with previous work.

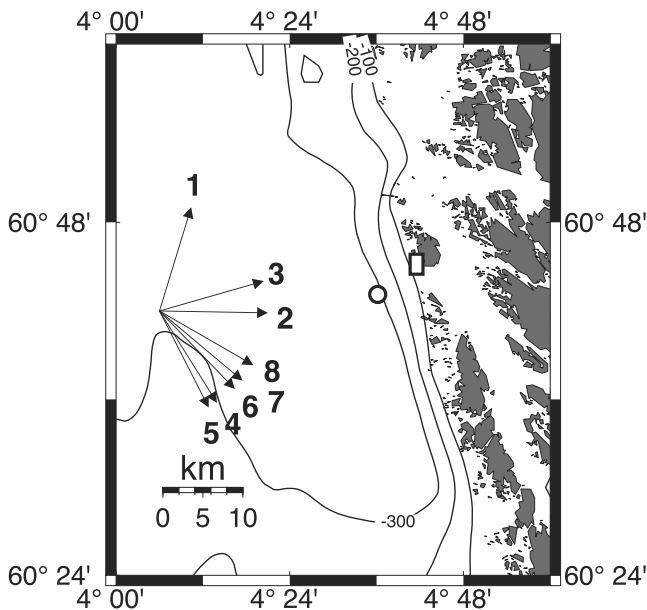


**Figure 11.** Bathymetry and coast line geometry near the buoy and radar system locations. The open circle marks the buoy position; the rectangle marks the location and geometrical configuration of the analysis window used by the X-band radar system enlarged by a factor of 2. The mean wave directions  $\varphi_m$  observed at the buoy (Table 1) are marked by arrows.

[52] During the measuring period, eight storms were observed which had significant wave height in excess of 5 m at the buoy position. The dominant generation areas have been located by means of three seismic arrays. For the strongest storm on 6/7 March (midnight), the southwest Norwegian coast has been identified as the generation area. From the width of the beam patterns an extent of about 500 km in north-south direction and less than 500 km in east-west direction has been estimated (Figure 8). Both the location and the extent of the generation area of this single storm agree well with the correlation map (Figure 6) representing an average over 34 days.

[53] Frequency analysis shows that the energy is concentrated at frequencies above 0.1 Hz (Figure 4), i.e., in the band of secondary microseisms. The theoretically predicted 1-to-2 relation between ocean wave and microseism frequencies is confirmed by comparing time series of peak frequencies (Figure 9) measured by the wave buoy off the southwest Norwegian coast and the seismic station in southern Norway (Kongsberg).

[54] The theory of the generation of secondary microseisms [Hasselmann, 1963] describes the microseism spectrum as a product of a transfer function, the extent of the generation area and the pressure spectrum at the seafloor, which is generated by nonlinear interactions between ocean surface waves. It is possible to determine the pressure spectrum by using radar measurements. Assuming that the unknown transfer function is independent of time, i.e., the special storm event, the relative extents of the generation areas can be estimated. It has been found that the linear dimensions of generation areas vary by a factor of less than 3.

[55] In summary, we conclude that during the experimental period the main generation area of microseisms was located near the southwest Norwegian coast. The extent along the coast is several 100 km and of the same order or less perpendicular to the coast. The microseism energy generated in this area is mainly controlled by the wave height. On the other hand, this means that relative ocean wave heights near the southwestern Norwegian coast can be estimated within about  $\pm 35\%$  from microseism spectral amplitudes.

[56] **Acknowledgments.** Thanks go to all institutions which provided the data: German Seismological Central Observatory SZGRF, Norwegian seismic Array NORSAR, Blacknest Data Center, and IRIS (microseism data), GKSS Research Center (wave buoy data), OceanSenseWare (radar data), German Weather Service DWD (wave model data). We thank Ed Sobel for reading the manuscript. Comments of two anonymous reviewers and the Associate Editor are gratefully acknowledged. The work was supported by the German Science Foundation DFG (Sonderforschungsbereich 512: Tiefdruckgebiete und Klimasystem des Nordatlantiks, Cyclones and the North Atlantic climate system).

## References

- Babcock, J. M., B. A. Kirkendall, and J. A. Orcutt, Relationships between Ocean Bottom Noise and the Environment, *Bull. Seismol. Soc. Am.*, **84**, 1991–2007, 1994.
- Bath, M., An investigation of the Uppsala microseisms, *Rep. 14*, 168 pp., Inst. of Meteorol., R. Univ. Uppsala, Uppsala, Sweden, 1949.
- Bromirski, P. D., Vibrations from the “Perfect Storm”, *Geochem. Geophys. Geosyst.*, **2**, Paper number 2000GC000119, 2001.
- Bromirski, P. D., and F. K. Duennebieer, The near-coastal microseism spectrum: Spatial and temporal wave climate relationships, *J. Geophys. Res.*, **107**(B8), 2166, doi:10.1029/2001JB000265, 2002.
- Bromirski, P. D., R. E. Flick, and N. Graham, Ocean wave-height determined from inland seismometer data: Implications for investigating wave climate changes in the NE Pacific, *J. Geophys. Res.*, **104**, 20,753–20,766, 1999.
- Bungum, H., E. Rygg, and L. Bruland, Short period seismic noise structure at the Norwegian seismic array, *Bull. Seismol. Soc. Am.*, **61**, 357–373, 1971.
- Bungum, H., S. Mykkeltveit, and T. Kvaerna, Seismic noise in Fennoscandia, with emphasis on high frequencies, *Bull. Seism. Soc. Amer.*, **75**, 1489–1513, 1985.
- Cessaro, R. K., Source of primary and secondary microseisms, *Bull. Seismol. Soc. Am.*, **84**, 142–156, 1994.
- Cessaro, R. K., and W. W. Chan, Wide angle triangulation array study of simultaneous primary microseism sources, *J. Geophys. Res.*, **94**, 15,555–15,563, 1989.
- Darbyshire, J., A further investigation of microseisms recorded in northern Wales, *Phys. Earth Planet. Inter.*, **67**, 330–347, 1991.
- Darbyshire, J., Microseisms formed off the coast of Norway, *Phys. Earth Planet. Inter.*, **73**, 282–289, 1992.
- Essen, H.-H., J. Klußmann, R. Herber, and I. Grevemeyer, Does microseisms in Hamburg (Germany) reflect the wave climate in the North Atlantic?, *Dtsch. Hydrogr. Z.*, **51**, 33–45, 1999.
- Friedrich, A., F. Krüger, and K. Klinge, Ocean-generated microseismic noise located with the GRFO array, *J. Seismol.*, **2**, 47–64, 1998.
- Friedrich, W., E. Wielandt, and S. Stange, Non plane geometries of seismic surface wavefields and their implications for regional surface-wave tomography, *Geophys. J. Int.*, **119**, 931–948, 1994.
- Grevemeyer, I., R. Herber, and H.-H. Essen, Microseismological evidence for a changing wave climate in the northeast Atlantic Ocean, *Nature*, **408**, 349–352, 2000.
- Gutenberg, B., Die seismische Bodenunruhe (in German), *Betr. Z. Geophys.*, **11**, 314–353, 1912.
- Gutenberg, B., *Untersuchungen über die Bodenunruhe mit Perioden von 4 s - 10 s in Europa* (in German), 106 pp., Veröff. de Zentralb. der Int. Seismol. Assoc., 1921.
- Gutenberg, B., On microseisms, *Bull. Seismol. Soc. Am.*, **26**, 111–117, 1936.
- Gutenberg, B., Microseisms and weather forecasting, *J. Meteorol.*, **4**, 21–28, 1947.
- Harjes, H. P., and M. Henger, Array seismology, *J. Geophys. Res.*, **39**, 865–905, 1973.
- Hasselmann, K., A statistical analysis of the generation of microseisms, *Rev. Geophys.*, **1**, 177–210, 1963.

- Haubrich, R. A., and K. McCamy, Microseisms: Coastal and pelagic sources, *Rev. Geophys.*, 7, 539–571, 1969.
- Kibblewhite, A. C., and K. C. Ewans, Wave-wave interactions, microseisms, and infrasonic ambient noise in the ocean, *J. Acoust. Soc. Am.*, 78, 981–994, 1985.
- Koch, K., and U. Kradolfer, Determination of mislocation vectors to evaluate bias at GSETT-3 primary stations, *J. Seismol.*, 3, 139–151, 1999.
- Komen, G. J., L. Cavaleri, M. Donelan, K. Hasselmann, S. Hasselmann, P. A. E. M. Janssen, *Dynamics and Modelling of Ocean Waves*, 532 pp., Cambridge Univ. Press, New York, 1994.
- Kvaerna, T., and F. Ringdahl, Stability of various f-k estimation techniques, in *Semiannual Technical Summary, 1 Oct. 1985 – 31 March 1986, NORSAR Sci. Rep. 1-86/87*, pp. 29–40, Kjeller, Norway, 1986.
- Longuet-Higgins, M. S., A theory of the origin of microseisms, *Philos. Trans. R. Soc. London, Ser. A*, 243, 1–35, 1950.
- Nieto Borge, J. C. N., K. Reichert, J. Dittmer, and C. T. Tindle, Use of nautical radar as a wave monitoring instrument, *Coastal Eng.*, 37, 331–342, 1999.
- Neidell, N. S., and T. Taner, Semblance and other coherency measures for multichannel data, *Geophysics*, 36, 482–497, 1971.
- Strobach, K., Ein Beitrag zum Problem der Entstehung und der Wellennatur der mikroseismischen Bodenunruhe (in German), *Hamburger Geophys. Einzelschrif.*, 5, 125 pp., Univ. Hamburg, Hamburg, Germany, 1962.
- Sutton, G. H., and N. Barstow, Ocean bottom microseisms from a distant supertyphoon, *Geophys. Res. Lett.*, 23, 499–502, 1996.
- Szelwis, R., Modeling of microseismic surface wave sources, *J. Geophys. Res.*, 87, 6906–6918, 1982.
- Webb, S. C., The equilibrium oceanic microseism spectrum, *J. Acoust. Soc. Am.*, 92, 2141–2158, 1992.
- Wiechert, E., Diskussion, Verhandlung der zweiten Internationalen Seismologischen Konferenz, Straßburg (in German), *Gerlands Beitr. Geophys.*, 2, 41–43, 1904.
- 
- T. Dahm, Institut für Geophysik, Universität Hamburg, Bundesstr. 55, D-20146 Hamburg, Germany. (dahm@dkrz.de)
- H.-H. Essen, Institut für Meereskunde, Universität Hamburg, Troplowitzstr. 7, D-22529 Hamburg, Germany. (essen@ifm.uni-hamburg.de)
- I. Grevemeyer, Fachbereich Geowissenschaften, Universität Bremen, Klagenfurter Straße, D-28359 Bremen, Germany. (ingo@geopys2.uni-bremen.de)
- F. Krüger, Institut für Geowissenschaften, Universität Potsdam, POB 601553, D-14415 Potsdam, Germany. (kruegerf@geo.uni-potsdam.de)